The Journal of Chemical Physics

RESEARCH ARTICLE | AUGUST 28 2020

A general automatic method for optimal construction of matrix product operators using bipartite graph theory

Jiajun Ren ; Weitang Li ; Tong Jiang ; Zhigang Shuai

Check for updates

J. Chem. Phys. 153, 084118 (2020)
https://doi.org/10.1063/5.0018149

View Online Export Citation

Articles You May Be Interested In

Optimal tree tensor network operators for tensor network simulations: Applications to open quantum systems

J. Chem. Phys. (August 2024)

Spectral coarse graining for random walks in bipartite networks

Chaos (January 2013)

Odd star decomposition of complete bipartite graphs

AIP Conf. Proc. (April 2020)

19 November 2025 14:41:53

Webinar From Noise to Knowledge

May 13th – Register now

Zurich Instruments Universität Konstanz

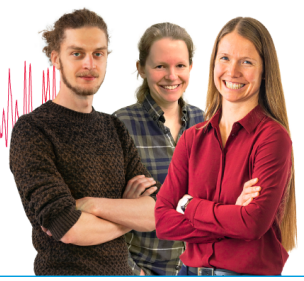

AIP Publishing

The Journal of Chemical Physics ARTICLE scitation.org/journal/jcp

A general automatic method for optimal construction of matrix product operators using bipartite graph theory

Cite as: J. Chem. Phys. 153, 084118 (2020); doi: 10.1063/5.0018149
Submitted: 12 June 2020 • Accepted: 12 August 2020 •
Published Online: 28 August 2020

View Online Export Citation CrossMark

Jiajun Ren,[a] Weitang Li, Tong Jiang, and Zhigang Shuai

AFFILIATIONS

MOE Key Laboratory of Organic OptoElectronics and Molecular Engineering, Department of Chemistry, Tsinghua University, Beijing 100084, People's Republic of China

[a]Author to whom correspondence should be addressed: renjj@mail.tsinghua.edu.cn

ABSTRACT

Constructing matrix product operators (MPOs) is at the core of the modern density matrix renormalization group (DMRG) and its time dependent formulation. For the DMRG to be conveniently used in different problems described by different Hamiltonians, in this work, we propose a new generic algorithm to construct the MPO of an arbitrary operator with a sum-of-products form based on the bipartite graph theory. We show that the method has the following advantages: (i) it is automatic in that only the definition of the operator is required; (ii) it is symbolic thus free of any numerical error; (iii) the complementary operator technique can be fully employed so that the resulting MPO is globally optimal for any given order of degrees of freedom; and (iv) the symmetry of the system could be fully employed to reduce the dimension of MPO. To demonstrate the effectiveness of the new algorithm, the MPOs of Hamiltonians ranging from the prototypical spin–boson model and the Holstein model to the more complicated *ab initio* electronic Hamiltonian and the anharmonic vibrational Hamiltonian with the sextic force field are constructed. It is found that for the former three cases, our automatic algorithm can reproduce exactly the same MPOs as the optimally hand-crafted ones already known in the literature.

Published under license by AIP Publishing. https://doi.org/10.1063/5.0018149

19 November 2025 14:41:53

I. INTRODUCTION

The density matrix renormalization group (DMRG) method originally proposed by White to solve the electronic structure of one-dimensional strongly correlated lattice models[1] has made great progress in quantum chemistry in the last decade and has been widely recognized as a state-of-the-art method for problems with a large active space.[2–9] In addition to the electronic correlation, the DMRG also shows great potential to solve the vibrational correlated problems.[10–12] More recently, the time dependent (TD) formulation of DMRG called TD-DMRG attracts a lot of attention and quickly emerges as an efficient and "nearly exact" method for quantum dynamics in complex systems. The TD-DMRG has been used to simulate the spectroscopy and quantum dynamics, including not only electron dynamics[13,14] but also electron-vibrational correlated dynamics.[15–22] For high-dimensional quantum dynamics, the multi-configuration time-dependent Hartree (MCTDH) method has long been considered as the gold standard.[23,24] However, it is limited by the exponential growth of computational cost with the system size—the curse of dimensionality. The multilayer MCTDH (ML-MCTDH) overcomes this limitation and has been successfully used to simulate the dynamics of model systems with thousands of degrees of freedom (DoF).[25] Like ML-MCTDH, the (TD-)DMRG could also achieve arbitrarily high accuracy with only polynomial computational effort. It has been demonstrated in a number of models with hundreds of DoFs to have the same accuracy as ML-MCTDH.[16–18,20,26]

The recent rapid advances in the quantum chemistry DMRG can be attributed to the formulation of DMRG as the matrix product state (MPS),[27] and the corresponding operator could be represented as a matrix product operator (MPO).[28] The introduction of MPS and MPO not only establishes a rigorous mathematical foundation of DMRG but also makes the algorithm more powerful and convenient.[29] Furthermore, it also opens the door to the

development of more general tensor network states (TNS), such as tree tensor network states (TTNS)[30,31] and projected entangled pair states (PEPS).[32] The DMRG is actually a special type of TNS with an one-dimensional matrix product ansatz, which is mathematically known as a tensor train (TT) format. Interestingly, from the TNS point of view, ML-MCTDH has a TTNS wavefunction ansatz with all physical DoF (primitive basis) at the leaf-node (lowest layer), which is mathematically called hierarchical Tucker format. In this sense, the ansatz of DMRG and the ansatz of ML-MCTDH are both low-rank approximations to the exact high-rank wavefunction, although historically they are independently developed in different research fields.[1,23,25] The modern formulation of the DMRG algorithm based on MPS and MPO is usually called the second generation DMRG algorithm,[33] which could be seamlessly combined with the variational principle to obtain the ground state and the time dependent variational principle to carry out the time propagation.[21,34] In addition, the exact global arithmetic, such as additions $\Psi_1 + \Psi_2$, $\hat{O}_1 + \hat{O}_2$ and multiplications $\hat{O}\Psi$, $\hat{O}_1\hat{O}_2$, is only possible based on MPS and MPO. In this new formulation, the starting point is to construct the MPO representation of the Hamiltonian and all the other required operators as an input to the rest DMRG calculations.

Generally speaking, there are two different types of operators. One is the analytical operator, such as the *ab initio* electronic Hamiltonian in quantum chemistry, the nuclear kinetic energy operator in an appropriate set of coordinates, and most of the physical and chemical model Hamiltonians. In addition, these analytical operators are commonly in a sum-of-products (SOP) form. The other type is the potential energy operator of real molecules met in the molecular nuclear Schrödinger equation. More specifically, the potential energy "operator" here is a complex N-dimensional potential energy surface (PES) $V(\boldsymbol{q}) = V(q_1, q_2, \ldots, q_N)$ and has no analytical forms. The potential energy (or energy derivative) at a specific structure $\boldsymbol{q}$ could be calculated by electronic structure calculation. For small-sized molecules with several atoms, very high accurate PESs are usually constructed globally by fitting and interpolating the available dataset of *ab initio* data points. The recent developed algorithm based on the neural network (NN) has made great progress in the direction.[35,36] For medium- and large-sized molecules, constructing full-dimensional global PESs is not even possible. The local PES around the equilibrium or saddle point could be expanded as a Taylor series with the high order energy derivatives. Although the Taylor expansion of PES has several known limitations such as that it could not describe double well potential and large amplitude motion, it is still very useful to calculate the anharmonic frequency of semi-rigid molecules and obtain a more accurate IR/Raman spectrum beyond the harmonic approximation.[37–39] For most numerical methods to solve the nuclear Schrödinger equation such as (ML-)MCTDH, one difficulty is to calculate the matrix element such as $\langle\Psi|V(\boldsymbol{q})|\Psi\rangle$, which is an N-dimensional quadrature problem. To reduce the cost, it is preferred to decompose the potential into an SOP form. In this way, the matrix elements could be calculated as a sum of product of N one-dimensional quadrature. The Taylor series expansion of the local potential apparently has an SOP form. For a general PES, Potfit[40] and the more efficient multigrid Potfit method[41] could decompose the PES numerically into a Tucker format from the energy grid points, which is suitable to the MCTDH calculation. The recently developed multilayer Potfit could integrate more effectively with ML-MCTDH.[42] Besides the Potfit-like methods, in the NN algorithm to fit the PES, if the activation function is an exponential function instead of the common hyperbolic tangent or sigmoid function, the NN with a single hidden layer also gives an analytical SOP form.[43] In addition to the SOP form, one of the other widely used methods to overcome the N-dimensional quadrature is called n-mode representation (n-MR) in which the PES is expanded as a sum of one-mode potential, two-mode potential, and so on, expecting that the series could converge with a small number of terms.[44] Thus, only low dimensional quadrature is needed. If necessary, each term in n-MR could be further fitted as sum-of-products of analytical functions such as polynomial and Morse types for each individual mode.[45] It is also worth mentioning that several methods could directly use the N-dimensional PES, such as the MCTDH combined with correlation discrete variable (CDVR) representation[46] and its multilayer generalization[47] proposed by Manthe and the collocation method proposed by Avila and Carrington.[48]

In this work, we focus on the construction of MPO for those operators that have an SOP form by definition or have been transformed into an SOP form by fitting a high-dimensional function (discrete points) as introduced above. For the same operator, the form of MPO could be completely different as long as the final product is correct. However, a more compact MPO will save computational cost in practice. In order to construct a compact MPO, several methods have been proposed. The most commonly used method in quantum chemistry is to design the MPO symbolically (or sometimes called analytically) by hand through inspecting the recurrence relation between neighboring sites.[49] The so-called complementary operator technique is always fully explored to make the MPO more compact, which is essential to the operators with long-range interactions,[50] such as the *ab initio* electronic Hamiltonian. Although usually this method could give the optimal answer by a smart design, it is not automatic in that different operators need a re-design and a re-implementation. The second one is a numerically "top-down" algorithm in which a naïve MPO is first constructed and then compressed by the singular value decomposition (SVD) or by removing the linearly dependent terms.[51] This algorithm is generic and automatic for different operators, while a numerical error is introduced and its effect on the following calculations cannot be well quantified in advance. Apart from this, the time cost spent on the numerical compression is not negligible when the number of terms in the operator is large. The third one, which is not widely used in quantum chemistry, is to construct a finite-state automaton to mimic the interaction terms in the operator.[28] The automaton is easy to be constructed for a translationally invariant lattice model with short-range interactions but becomes extremely complicated for long-range interactions.

Unlike the *ab initio* electronic Hamiltonian that has the same formula for different systems and thus could be hard-coded in implementation, a general Hamiltonian could be completely different according to the different interactions within the system. Thus, it is not efficient to use the first hand-crafting method mentioned above to construct MPOs on a case-by-case basis. In addition to the inefficiency, it is also difficult to obtain a globally optimal MPO when the Hamiltonian is very complicated. Therefore, it is necessary and desired to have a better MPO construction algorithm that has all the advantages of the methods introduced above: (i) it is generic for all

19 November 2025 14:41:53

Published under license by AIP Publishing

types of operators with an analytical SOP form; (ii) it is automatic, directly from the symbolic operator strings to the MPO; and (iii) it gives an optimal MPO. Here, "optimal" means that the MPO is as compact as possible globally in a given order of DoF. (iv) It is symbolic thus free of any numerical error. In this work, we propose a new MPO construction algorithm that meets all the four requirements based on the graph theory for a bipartite graph. The remaining sections of this paper are arranged as follows: In Sec. II, we will present the idea of the new algorithm and the implementation details. In Sec. III, several typical Hamiltonians are examined ranging from the simple spin–boson model and the Holstein model to the more complicated *ab initio* electronic Hamiltonian and the vibrational Hamiltonian described by a sextic force field. All the calculations are carried out with our in-house code Renormalizer.[52] The resulting MPOs are compared with the optimally hand-crafted ones reported in the literature.

II. METHODOLOGY AND IMPLEMENTATION

A. MPO and complementary operator technique

The wavefunction ansatz in the DMRG is called the matrix product states or tensor train, which is

$$|\Psi\rangle = \sum_{\{a\},\{\sigma\}} A[1]^{\sigma_1}_{a_1} A[2]^{\sigma_2}_{a_1 a_2} \cdots A[N]^{\sigma_N}_{a_{N-1}} |\sigma_1 \sigma_2 \cdots \sigma_N\rangle. \tag{1}$$

For a system of distinguishable particles, N is the number of DoFs in the system, and $\{|\sigma_i\rangle\}$ is the local basis such as the discrete variable representation (DVR) basis for nuclear motion. For electronic systems, N is the number of orbitals, and $\{|\sigma_i\rangle\}$ is the occupation configuration of each orbital (if using spatial-orbital, $\{|\sigma_i\rangle\} = \{|\text{vacuum}\rangle, |\uparrow\rangle, |\downarrow\rangle, |\uparrow\downarrow\rangle\}$; if using spin-orbital, $\{|\sigma_i\rangle\} = \{|\text{vacuum}\rangle, |\text{occupied}\rangle\}$). $\{A[i]^{\sigma_i}_{a_{i-1}a_i}\}$ are the local matrices connected by the indices a_i, which is commonly called (virtual) bond with bond dimension M_S or denoted as $|a_i|$. σ_i is called the physical bond with dimension d. One good feature of DMRG is that the accuracy is only determined by the dimension of the virtual bond and thus could be systematically improved.

Similar to the MPS, any operator $\hat{O}$ could be expressed as a matrix product operator,[29,49]

$$\hat{O} = \sum_{\{w\},\{\sigma\},\{\sigma'\}} W[1]^{\sigma_1',\sigma_1}_{w_1} W[2]^{\sigma_2',\sigma_2}_{w_1 w_2} \cdots W[N]^{\sigma_N',\sigma_N}_{w_{N-1}} \times |\sigma_1' \sigma_2' \cdots \sigma_N'\rangle\langle\sigma_N \sigma_{N-1} \cdots \sigma_1|. \tag{2}$$

The MPO could be constructed by sequential singular value decompositions from the matrix element representation $\mathbf{O}_{\sigma_1'\sigma_2'\cdots\sigma_N',\sigma_1\sigma_2\cdots\sigma_N}$, numerically, but it is not practical for a large system since the exact decomposition needs the bond dimension M_O to increase exponentially, which is $d^2, d^4, \ldots, d^{N-2}, d^N, d^{N-2}, \ldots, d^2$ if N is even. In practice, if an operator has an SOP form, the MPO is usually first constructed symbolically,

$$\hat{O} = \sum_{\{z\}} \gamma_{z_1 z_2 \cdots z_N} \hat{z}_1 \hat{z}_2 \cdots \hat{z}_N \tag{3}$$

$$= \sum_{\{w\},\{z\}} W[1]^{z_1}_{w_1} W[2]^{z_2}_{w_1 w_2} \cdots W[N]^{z_N}_{w_{N-1}} \hat{z}_1 \hat{z}_2 \cdots \hat{z}_N \tag{4}$$

$$= \sum_{\{w\}} \hat{W}[1]_{w_1} \hat{W}[2]_{w_1 w_2} \cdots \hat{W}[N]_{w_{N-1}}. \tag{5}$$

In Eq. (3), $\{\hat{z}_i\}$ represents the elementary operators of each local site such as $\{\hat{I}, \hat{p}^2, \hat{x}, \hat{x}^2, f(\hat{x}, \hat{p}), \text{etc.}\}$ for a vibrational site or $\{\hat{I}, \hat{a}^\dagger, \hat{a}, \hat{a}^\dagger\hat{a}\}$ for an electronic site. The prefactor $\gamma_{z_1 z_2 \cdots z_N}$ is commonly very sparse. For example, in the *ab initio* electronic Hamiltonian, $\gamma_{z_1 z_2 \cdots z_N} = 0$, if more than four $\hat{z}_i$ are $\hat{a}^\dagger$ or $\hat{a}$. $\gamma_{z_1 z_2 \cdots z_N}$ could be regarded as the coefficient of $\hat{O}$ on the operator basis $\hat{z}_1 \hat{z}_2 \cdots \hat{z}_N$, and its matrix product representation in Eq. (4) is very similar to an MPS in Eq. (1). In Eq. (5), $\hat{W}[i] = \sum_{z_i} W[i]^{z_i} \hat{z}_i$ is a matrix composed of some prefactor attached symbolic operators acting locally on site i. From this symbolic MPO, it is easy to obtain the matrix element representation as Eq. (2) by expanding $\hat{W}[i]$ on the local basis $\{|\sigma_i\rangle\}$.

From $\gamma_{z_1 z_2 \cdots z_N}$, if all terms with a nonzero prefactor are extracted, $\hat{O}$ can also be expressed as

$$\hat{O} = \sum_{o=1}^{K} \hat{O}[1:N]_o = \sum_{o=1}^{K} \left(\gamma_o \prod_{i=1}^{N} \hat{z}_i^o \right). \tag{6}$$

K is the number of nonzero terms in total. $\hat{z}_i^o$ is the local operator of the oth term at site i and could be any of the elementary operators in $\{\hat{z}_i\}$. The slice $[1{:}N]$ indicates that the operator is from site 1 to site N. The MPO representation of each term $\hat{O}[1{:}N]_o$ in Eq. (6) has $M_O = 1$ with $\hat{W}[i] = \hat{z}_i^o$, and the prefactor γ_o could be attached to any site. The global arithmetic addition of any two MPOs (not necessary to have $M_O = 1$) is

$$\gamma_1 \hat{O}[1:N]_1 + \gamma_2 \hat{O}[1:N]_2 = \begin{bmatrix} \hat{z}_1^1 & \hat{z}_1^2 \end{bmatrix} \left(\prod_{i=2}^{N-1} \begin{bmatrix} \hat{z}_i^1 & \mathbf{0} \\ \mathbf{0} & \hat{z}_i^2 \end{bmatrix} \right) \begin{bmatrix} \gamma_1 \hat{z}_N^1 \\ \gamma_2 \hat{z}_N^2 \end{bmatrix}, \tag{7}$$

which merges the local matrices block-diagonally. Therefore, the naïve way to construct the MPO of $\hat{O}$ in Eq. (6) will give $M_O = K$.

A more systematic way to derive the MPO is to use the recurrence relation between the neighboring sites. When the system is split between site i and site $i+1$ into the respective left (L, from site 1 to i) and right (R, from site $i+1$ to N) blocks, $\hat{O}$ could be expressed as

$$\hat{O} = \sum_{o_i=1}^{K} \gamma_{o_i} \cdot \hat{O}[1:i]_{o_i} \otimes \hat{O}[i+1:N]_{o_i}, \tag{8}$$

where $\hat{O}[1:i]_{o_i} = \prod_{j=1}^{i} \hat{z}_j^{o_i}$ and $\hat{O}[i+1:N]_{o_i} = \prod_{j=i+1}^{N} \hat{z}_j^{o_i}$ are usually called the normal operators. A recurrence relation between the neighboring $\hat{O}[1:i-1]_{o_{i-1}}$ and $\hat{O}[1:i]_{o_i}$ could be defined as

$$\hat{O}[1:i]_{o_i} = \sum_{o_{i-1}=1}^{K} \hat{O}[1:i-1]_{o_{i-1}} \hat{O}[i]_{o_{i-1} o_i} \tag{9}$$

from which the symbolic MPO in Eq. (5) could be obtained directly with $\hat{W}[i] = \hat{O}[i]$ and again the prefactor γ_{o_i} could be attached to any

19 November 2025 14:41:53

Published under license by AIP Publishing

site. This construction gives the same result as the global arithmetic addition of K MPOs with $M_O = 1$ in Eq. (7). However, it is apparently not optimal in that some of the interaction terms in Eq. (8) may share the common operators in the set $\{\hat{O}[1:i]_{o_i}\}$ or $\{\hat{O}[i+1:N]_{o_i}\}$. For example, if $K = 2$ and $\hat{O}[i+1:N]_1 \equiv \hat{O}[i+1:N]_2$, while $\hat{O}[1:i]_1 \neq \hat{O}[1:i]_2$, $\hat{O}[1:i]_1$ and $\hat{O}[1:i]_2$ could be summed up with the prefactors to create a complementary operator $\hat{\tilde{O}}[1:i]_1 = \gamma_1\hat{O}[1:i]_1 + \gamma_2\hat{O}[1:i]_2$ on the L-block, and meanwhile, $\hat{O}[i+1:N]_2$ is removed from the R-block so that $\hat{O} = \hat{\tilde{O}}[1:i]_1 \otimes \hat{O}[i+1:N]_1$. Thus, $|o_i|$, the number of columns of $\hat{O}[i]$ is reduced by 1. This example shows that the MPO representation of the same operator is not unique as long as the product result is correct. Generally speaking, to make the MPO compact, if there are redundant operators in $\{\hat{O}[i+1:N]_{o_i}\}(\{\hat{O}[1:i]_{o_i}\})$, the corresponding left (right) complementary operators could be created. This complementary operator technique[50] is of essential importance in constructing the MPO for the *ab initio* electronic Hamiltonian by assembling all the 4-index operators $\sum_{pqrs} g_{pqrs}a_p^\dagger a_q^\dagger a_r a_s$ and 3-index operators $\sum_{pqr} g_{pqrs}a_p^\dagger a_q^\dagger a_r$ and part of the 2-index operators in one block, reducing M_O from $\mathcal{O}(N^4)$ to $\mathcal{O}(N^2)$.[33,49] However, the complexity of designing complementary operators comes from that in most Hamiltonians, both $\hat{O}[1:i]_{o_i}$ and $\hat{O}[i+1:N]_{o_i}$ in one interaction term are correlated with other interaction terms. For instance, we add another two terms in the former example, $\hat{O}[1{:}i]_1 \equiv \hat{O}[1{:}i]_3$ and $\hat{O}[1{:}i]_2 \equiv \hat{O}[1{:}i]_4$. In this case, the optimal solution is to create complementary operators $\hat{\tilde{O}}[i+1:N]_1 = \gamma_1\hat{O}[i+1:N]_1 + \gamma_3\hat{O}[i+1:N]_3$ and $\hat{\tilde{O}}[i+1:N]_2 = \gamma_2\hat{O}[i+1:N]_2 + \gamma_4\hat{O}[i+1:N]_4$, which will give $|o_i| = 2$. While creating the complementary operator $\hat{\tilde{O}}[1:i]_1$ as above will result in $|o_i| = 3$. This toy example shows that the design of complementary operators is nontrivial. A typical real example is that when constructing the MPO of the *ab initio* electronic Hamiltonian, a different design strategy of the complementary operators of the 2-index operators within one block will lead to a different M_O shown in Fig. 10 of Ref. 49, though all of them are $\mathcal{O}(N^2)$. Therefore, the key to construct a compact MPO is to design and select the normal and complementary operators smartly at each bond to make the number of retained operators as small as possible. As far as we know, up to now it is still an art to design the complementary operators by hand on a case-by-case basis rather than by a rigorous and automatic procedure.

B. MPO construction algorithm via bipartite graph theory

We propose to use the theory of bipartite graph to set a rigorous foundation to construct the MPO automatically. We first reinterpret the operator selection problem at each bond mentioned in Sec. II A as a minimum vertex cover problem in a bipartite graph and then prove that the locally optimal solution is also globally optimal.

The non-redundant operator set by removing the duplicated operators in $\{\hat{O}[1:i]_{o_i}\}, \{\hat{O}[i+1:N]_{o_i}\}$ of Eq. (8) is denoted as $U = \{\hat{U}[1:i]_{u_i}\}, V = \{\hat{V}[i+1:N]_{v_i}\}$, which are represented as the vertices in Fig. 1. Unlike that the interaction pattern is one-to-one between $\{\hat{O}[1:i]_{o_i}\}$ and $\{\hat{O}[i+1:N]_{o_i}\}$, it would be one-to-many between $\{\hat{U}[1:i]_{u_i}\}$ and $\{\hat{V}[i+1:N]_{v_i}\}$. The K interaction terms are represented as the edges denoted as E each connecting one vertex in U to one vertex in V with a prefactor (weight) $\gamma_{u_i v_i}$. A bipartite graph is often denoted as $G = (U, V, E)$. If the pth vertex in U is selected, the corresponding operator $\hat{U}[1{:}i]_p$ in the L-block is retained. Meanwhile, the operators $\hat{V}[i+1:N]_q$ corresponding to the vertices in V, which are linked to $\hat{U}[1{:}i]_p$ through edges, are multiplied by the prefactor of the certain edge and then are added up to create a new complementary operator in the R-block $\sum_q \gamma_{pq}\hat{V}[i+1:N]_q$. The same rule is applied if a vertex in V is selected. Therefore, the minimal number of retained operators in one block, which could cover all the K interaction terms, is equal to the minimal number of selected vertices in (U, V), which could cover all the edges in E (shown in blue in Fig. 1). The latter problem is called the minimum vertex cover in graph theory. For a bipartite graph described here, the König theorem proves that the number of vertices in the minimum vertex cover is equal to the number of edges in the maximum matching.[53] A matching is an edge set in which any two edges do not share one vertex. The maximum matching shown in red in Fig. 1 is the matching having the maximal number of edges, which could be solved efficiently by the Hungarian algorithm[54] with complexity $\mathcal{O}(nm)$ or the Hopcroft–Karp algorithm[55] with complexity $\mathcal{O}(\sqrt{n}m)$ through finding an augmenting path.[53] Here, n and m are the total number of vertices and edges in the bipartite graph, respectively. Once the maximum matching is found, the vertices in the minimum vertex cover could be obtained easily, and the retained operators are optimally selected according to the rules above.

For a DMRG chain with a certain order, the whole procedure to construct the MPO of $\hat{O}$ from site 1 to N (from N to 1 is similar) is summarized as follows:

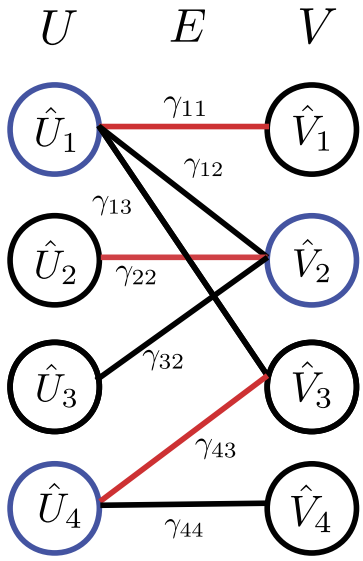

FIG. 1. An example of mapping the operator $\hat{O} = \gamma_{11}\hat{U}_1\hat{V}_1 + \gamma_{12}\hat{U}_1\hat{V}_2 + \gamma_{13}\hat{U}_1\hat{V}_3 + \gamma_{22}\hat{U}_2\hat{V}_2 + \gamma_{32}\hat{U}_3\hat{V}_2 + \gamma_{43}\hat{U}_4\hat{V}_3 + \gamma_{44}\hat{U}_4\hat{V}_4$ to a bipartite graph $G = (U, V, E)$. The vertices represent the non-redundant operators in the L- and R-block. The edges represent the interactions with a nonzero prefactor. The vertices in blue form a minimum vertex cover. The edges in red form a maximum matching.

19 November 2025 14:41:53

Published under license by AIP Publishing

1. The incoming non-redundant operator set of site i is known as $\{\hat{W}[1:i-1]_{w_{i-1}}\}$ ($\{\hat{W}[1{:}0]\}$ is $\{1\}$), which are also the outgoing operators of site $i-1$. Commonly, $\{\hat{W}[1:i-1]_{w_{i-1}}\}$ includes both normal operators and complementary operators. Next, $\{\hat{W}[1:i-1]_{w_{i-1}}\}$ is multiplied by the local elementary operators $\{\hat{z}_i\}$ on site i to form a non-redundant operator set $\{\hat{U}[1:i]_{u_i}\} = \{\hat{W}[1:i-1]_{w_{i-1}}\} \otimes \{\hat{z}_i\}$. The R-block non-redundant operator set is $\{\hat{V}[i+1:N]_{v_i}\}$ in which all operators are normal operators. Note that for efficiency, only the interaction terms with a nonzero prefactor are necessary to be included in the operator sets $\{\hat{U}[1:i]_{u_i}\}$ and $\{\hat{V}[i+1:N]_{v_i}\}$. Hence, at this boundary between site i and $i+1$, $\hat{O} = \sum_{u_i v_i} \gamma_{u_i v_i} \hat{U}[1:i]_{u_i} \otimes \hat{V}[i+1:N]_{v_i}$.
2. The operators in $\{\hat{U}[1:i]_{u_i}\}$, $\{\hat{V}[i+1:N]_{v_i}\}$ and the interactions between them are represented as vertices and edges to form a bipartite graph $G = (U, V, E)$ (see Fig. 1). Afterward, the maximum matching and the corresponding minimum vertex cover of this bipartite graph are found with the Hungarian algorithm or the Hopcroft–Karp algorithm. Next, iterating through each vertex in the minimum vertex cover once:
   2.1. If the vertex is the pth vertex in U, the operator $\hat{U}[1{:}i]_p$ is retained, and meanwhile, the edges linked to it are removed from the graph.
   2.2. If the vertex is the qth vertex in V, the complementary operator linked through edges to $\hat{V}[i+1:N]_q$ is created and retained, which is $\hat{\tilde{U}}[1:i]_q = \sum_p \gamma_{pq} \hat{U}[1:i]_p$. Meanwhile, the edges are removed.

   The reason to remove the edges after each visit is to avoid the double-counting of the interactions. After all the vertices in the minimum vertex cover are visited once, there will be no edge in the graph.
3. The retained operators $\hat{U}[1{:}i]_p$ and $\hat{\tilde{U}}[1:i]_q$ together form a new non-redundant operator set $\{\hat{W}[1:i]_{w_i}\}$ in the L-block. It is the outgoing operator set of site i and meanwhile is the incoming operator set of site $i+1$. After that, with $\{\hat{W}[1:i-1]_{w_{i-1}}\}$ and $\{\hat{W}[1:i]_{w_i}\}$, the local symbolic MPO $\hat{W}[i]$ is easy to obtain according to the recurrence relation $\hat{W}[1{:}i] = \hat{W}[1{:}i-1]\hat{W}[i]$. In fact, the local prefactor matrix $W[i]^{z_i}_{w_{i-1}w_i}$ in $\hat{W}[i]_{w_{i-1}w_i} = \sum_{z_i} W[i]^{z_i}_{w_{i-1}w_i}\hat{z}_i$ is the transformation matrix (reshaped to be $W[i]_{w_{i-1}z_i,w_i}$) of operator basis from $\{\hat{W}[1:i-1]_{w_{i-1}}\} \otimes \{\hat{z}_i\}$ to $\{\hat{W}[1:i]_{w_i}\}$.
   Return back to step 1.

The procedure described above is apparently a locally optimal solution, since the selected operators have already been the minimum vertex cover at each boundary when sweeping from left to right. To prove that the locally optimal solution is also globally optimal, we should prove that at each boundary between site i and $i+1$, the number of edges in the maximum matching (the number of vertices in the minimum vertex cover) is the same no matter whether the operator set of L-block is composed of all normal operators or is composed of both normal operators and complementary operator as $\{\hat{W}[1:i]_{w_i}\}$ according to steps 1–3. Following Eq. (3), if the coefficient tensor $\gamma_{z_1 z_2 \cdots z_N}$ is reshaped as a matrix $\gamma_i = \gamma_{z_1 z_2 \cdots z_i, z_{i+1} \cdots z_N}$, it could be regarded as the coefficient matrix of $\hat{O}$ expanded on the operator basis $\{\hat{z}_1 \otimes \cdots \otimes \hat{z}_i\} \otimes \{\hat{z}_{i+1} \otimes \cdots \otimes \hat{z}_N\}$ in the operator space. γ_i is called the unfolding matrix of γ in Ref. 56 whose rank is denoted as r_i called TT-rank. The bipartite graph $G[i] = (U[i], V[i], E[i])$ at the boundary between site i and site $i+1$ is $U[i] = \{\hat{z}_1 \otimes \cdots \otimes \hat{z}_i\}$, $V[i] = \{\hat{z}_{i+1} \otimes \cdots \otimes \hat{z}_N\}$, and the edges $E[i]$ have a one-to-one correspondence to the nonzero matrix elements in γ_i. In the bipartite graph theory, the matrix γ_i could also be regarded as a symbolic bipartite adjacency matrix for which only that the matrix elements are zero or nonzero is important. Lovász proposed the theorem that the rank of the symbolic adjacency matrix is equal to the number of edges of a maximum matching.[57] Therefore, since $U[i]$ and $V[i]$ are composed of all normal operators, using the rules described above to select the normal and complementary operators, the ideally minimal number of retained operators at this boundary is equal to r_i, the rank of matrix γ_i. In the Appendix, we prove that sweeping from left to right as the procedure above will not change the rank of the adjacency matrix at the same boundary. It is worth noting that in Ref. 51, the ideal rank r_i of MPO at the ith bond is expected to be approached by numerical SVD compression, deparallelization, and delinearization, but it is not guaranteed because of the numerical error. However, here, it is guaranteed symbolically via the bipartite graph theory. In addition, the scaling of the current algorithm is roughly $\mathcal{O}(K^{3/2}N)$ with the Hopcroft–Karp algorithm. In comparison, the scaling of the SVD-based algorithm is roughly $\mathcal{O}(K^3 d^2 N)$. Thus, the current algorithm is much cheaper.

Several other advantages of the algorithm are that (i) the sparsity of MPO is fully maintained, which could be used to reduce the computational cost during the tensor contraction in DMRG single state or time evolution algorithms. (ii) The symmetry could be directly implemented by attaching the good quantum numbers on each normal and complementary operator. (iii) The algorithm not only works for MPO construction but also works for MPS construction if the wavefunction in the Fock space representation has already been known. For the same reason, the obtained MPS is the most compact one to represent the wavefunction exactly.

Finally, it should be mentioned that for a system in which the interaction pattern is inhomogeneous, the order of DoFs will affect the size of MPO. It is still unclear whether there is an algorithm, which could efficiently find out a specific order giving the minimal MPO. However, in our opinion, this problem is less of a priority than the widely known ordering problem with respect to the accuracy of DMRG calculation.[58,59]

III. RESULTS

In this section, we will demonstrate the effectiveness of the new algorithm by constructing the MPOs of Hamiltonians ranging from the simple spin–boson model and the Holstein model to the more complicated *ab initio* electronic Hamiltonian and the vibrational Hamiltonian with a sextic force field.

A. Spin–boson model and Holstein model

The spin–boson model [expressed in the first quantization formalism in Eq. (10)] describes a two-level system coupled with a harmonic bath, which is widely used to investigate the quantum

19 November 2025 14:41:53

Published under license by AIP Publishing

dissipation,

$$\hat{H}_{\mathrm{SBM}} = \varepsilon\hat{\sigma}_z + \Delta\hat{\sigma}_x + \frac{1}{2}\sum_i(\hat{p}_i^2 + \omega_i^2\hat{q}_i^2) + \hat{\sigma}_z\sum_i c_i\hat{q}_i. \tag{10}$$

The Holstein model [expressed in the second quantization formalism in Eq. (11)] is also a widely used electron-vibrational coupling model to describe the charge transport, energy transfer, and spectroscopy of molecular aggregates.[17,21,22,60,61] It could be regarded as a group of two-level systems as the spin–boson model coupled with each other through coupling constant J_{ij},

$$\hat{H}_{\mathrm{Holstein}} = \sum_i \varepsilon_i a_i^\dagger a_i + \sum_{i\neq j} J_{ij} a_i^\dagger a_j + \sum_{in}\omega_{in} b_{in}^\dagger b_{in} + \sum_{in}\omega_{in} g_{in} a_i^\dagger a_i (b_{in}^\dagger + b_{in}). \tag{11}$$

Both of the two models are often adopted to benchmark the quantum dynamics methods. We put the two models in the same section because the spin–boson model could be regarded as a one-site Holstein model with an additional interstate coupling Δ, and thus, the MPOs of them are very similar. We test a spin–boson model with 100 discrete modes and the order is [spin, ν_1, ν_2, …, ν_{100}]. We also test two Holstein models with 20 electronic sites and both of them have two vibrational modes of each electronic site, but the former only has one-dimensional nearest-neighbor electronic hopping, while the latter has long-range hoppings between any two electronic sites. The order of the Holstein model is [e_1, $\nu_{1,1}$, $\nu_{1,2}$, e_2, $\nu_{2,1}$, $\nu_{2,2}$, …, e_{20}, $\nu_{20,1}$, $\nu_{20,2}$]. The MPO bond dimension M_O vs the bond index is shown in Fig. 2. The reference results (blue line) are based on a hand-crafted strategy in which the normal operators for the electronic coupling terms are switched to the complementary operators $\hat{P}_j = \sum_i J_{ij}a_i$ and $\hat{P}_j^\dagger = \sum_i J_{ij}a_i^\dagger$ after passing the middle electronic site. The details are provided in the Appendix in our former work,[17] which is believed to be near-optimal for the two models (from the results shown below, it is optimal except at the first bond for the Holstein model).

For the spin–boson model shown in Fig. 2(a), M_O is a constant independent of system size because $\hat{W}[1:i] = \{\hat{H}[1:i], \hat{\sigma}_z, \hat{I}\}$, where $\hat{H}[1{:}i]$ is the complete Hamiltonian from site 1 to i. The new automatic algorithm gives exactly the same result as the hand-crafted one. For the Holstein model shown in Figs. 2(b) and 2(c), M_O is independent of the number of the electronic site when the electronic coupling is one-dimensional nearest-neighbor coupling, while it is linearly dependent on the number of the electronic site if the long-range hopping is allowed. The new automatic algorithm gives the same results as the hand-crafted ones, except at the first bond, where the new algorithm gives one less bond dimension. This minor difference comes from that the hand-crafted strategy gives $\hat{W}[1] = \{\varepsilon_1 a_1^\dagger a_1, a_1^\dagger a_1, a_1^\dagger, a_1, \hat{I}\}$, while the automatic algorithm gives $\hat{W}[1] = \{a_1^\dagger a_1, a_1^\dagger, a_1, \hat{I}\}$ and the local energy of the first site $\varepsilon_1 a_1^\dagger a$ is considered in $\hat{W}[2]_{0,0} = \varepsilon_1\hat{I}$. Although this small improvement will not make a noticeable difference on the actual computational cost, it is clear to demonstrate that since the new algorithm is globally optimal, it could find out the redundancy, which will be neglected sometimes with the common hand-crafted strategy.

B. *Ab initio* electronic Hamiltonian

The second Hamiltonian considered is the *ab initio* electronic Hamiltonian in which up to 4 sites interact with each other. Thus, it is much more complicated than the spin–boson model and Holstein model. With spin-orbitals, the Hamiltonian is written as

$$\hat{H}_{\mathrm{el}} = \sum_{p,q=1}^{N} h_{pq}a_p^\dagger a_q + \frac{1}{2}\sum_{p,q,r,s=1}^{N} v_{pqrs}a_p^\dagger a_q^\dagger a_r a_s = \sum_{p,q=1}^{N} h_{pq}a_p^\dagger a_q + \sum_{p<q,r<s}^{N} g_{pqrs}a_p^\dagger a_q^\dagger a_r a_s, \tag{12}$$

where the two-electron integral v_{pqrs} is $(ps|qr)$ in chemist's notation. The second equality takes advantage of the symmetry in v_{pqrs} ($g_{pqrs} = v_{pqrs} - v_{qprs} = v_{pqrs} - v_{pqsr}$).

First, we introduce the optimal hand-crafted strategy to construct the MPO of the *ab initio* electronic Hamiltonian. For more implementation details, refer to Ref. 49. For convenience, $\hat{H}_{\mathrm{el}}$ is divided into three components. The first part is $\hat{H}_1 = \hat{H}_L + \hat{H}_R$ in which $\hat{H}_L$ and $\hat{H}_R$ are the full Hamiltonian of the orbitals in the L-block and R-block, respectively. In fact, $\hat{H}_L$ and $\hat{H}_R$ could be

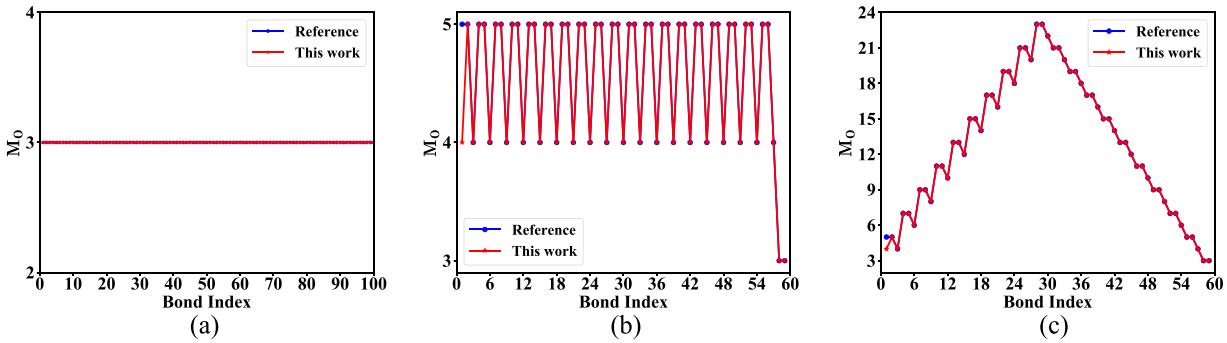

FIG. 2. The bond dimension M_O vs the bond index in (a) the spin–boson model with 100 discrete vibrational modes. (b) The Holstein model of 20 electronic sites with only one-dimensional electronic coupling and each electronic site has two vibrational modes. (c) The same as in (b), except with arbitrary long-range electronic couplings. The reference results (blue line) are based on the hand-crafted complementary operator strategy provided in our former work.[17]

19 November 2025 14:41:53

Published under license by AIP Publishing

regarded as the complementary operators of identity operator $\hat{I}_R$ and $\hat{I}_L$ in the R-block and L-block, reducing $\mathcal{O}(N^4)$ normal operators to one complementary operator. Apparently, $\hat{H}_1$ gives $M_{O,1} = 2$ at each bond. The second part with two fermionic creation or annihilation (elementary) operators in each block is written as

$$\hat{H}_2 = \sum_{p<q,r<s} -g_{p_L q_R r_L s_R}\left(a^\dagger_{p_L} a_{r_L}\right)\left(a^\dagger_{q_R} a_{s_R}\right) + g_{p_L q_L r_R s_R}\left(a^\dagger_{p_L} a^\dagger_{q_L}\right)\left(a_{r_R} a_{s_R}\right) + g_{p_R q_R r_L s_L}\left(a_{r_L} a_{s_L}\right)\left(a^\dagger_{p_R} a^\dagger_{q_R}\right). \quad (13)$$

The optimal strategy to design the complementary operator depends on the number of orbitals denoted as n_L and n_R in each block. For instance, if $n_L > n_R$, the complementary operators of the first term in Eq. (13) are $\hat{P}_{qs} = \sum_{pr} -g_{p_L q_R r_L s_R}\left(a^\dagger_{p_L} a_{r_L}\right)$, which have n_R^2 terms in total. Therefore, the ideally minimal bond dimension is $M_{O,2} = \min(n_L^2, n_R^2) + 2 \cdot \min(n_L(n_L-1)/2, n_R(n_R-1)/2)$. The third part with one creation or annihilation operator in one block and three in the other is commonly written as

$$\begin{aligned}\hat{H}_3 = &\sum_p a^\dagger_{p_L}\left(\sum_q \frac{1}{2} h_{p_L q_R} a_{q_R} + \sum_{qrs} g_{p_L q_R r_R s_R} a^\dagger_{q_R} a_{r_R} a_{s_R}\right)\\ &+ \sum_r a_{r_L}\left(\sum_s -\frac{1}{2} h_{s_R r_L} a^\dagger_{s_R} + \sum_{pqs} g_{p_R q_R r_L s_R} a^\dagger_{p_R} a^\dagger_{q_R} a_{s_R}\right)\\ &+ \sum_q\left(\sum_p -\frac{1}{2} h_{q_R p_L} a_{p_L} + \sum_{psr} g_{p_L q_R r_L s_L} a^\dagger_{p_L} a_{r_L} a_{s_L}\right) a^\dagger_{q_R}\\ &+ \sum_s\left(\sum_r \frac{1}{2} h_{r_L s_R} a^\dagger_{r_L} + \sum_{pqr} g_{p_L q_L r_L s_R} a^\dagger_{p_L} a^\dagger_{q_L} a_{r_L}\right) a_{s_R}. \end{aligned} \quad (14)$$

The terms in the parentheses are the complementary operators, which should be first summed up. This kind of complementary operator is adopted to construct the MPO of the *ab initio* electronic Hamiltonian because it greatly reduces $M_{O,3}$ from $\mathcal{O}(N^3)$ to $\mathcal{O}(N)$. However, it is only near-optimal because near the left boundary of the chain, there are more 1-index operators in the R-block than 3-index operators in the L-block. Thus, the optimal way to construct the complementary operator at this boundary is

$$\begin{aligned}\hat{H}_3 = &\sum_p a^\dagger_{p_L}\left(\sum_q h_{p_L q_R} a_{q_R} + \sum_{qrs} g_{p_L q_R r_R s_R} a^\dagger_{q_R} a_{r_R} a_{s_R}\right)\\ &+ \sum_r a_{r_L}\left(\sum_s -h_{s_R r_L} a^\dagger_{s_R} + \sum_{pqs} g_{p_R q_R r_L s_R} a^\dagger_{p_R} a^\dagger_{q_R} a_{s_R}\right)\\ &+ \sum_{prs} a^\dagger_{p_L} a_{r_L} a_{s_L}\left(\sum_q g_{p_L q_R r_L s_L} a^\dagger_{q_R}\right)\\ &+ \sum_{pqr} a^\dagger_{p_L} a^\dagger_{q_L} a_{r_L}\left(\sum_s g_{p_L q_L r_L s_R} a_{s_R}\right). \end{aligned} \quad (15)$$

The case is the same near the right boundary of the chain. Therefore, the minimal $M_{O,3}$ equals $2 \cdot \min(n_L^2(n_L-1)/2, n_R) + 2 \cdot \min(n_L, n_R^2(n_R-1)/2)$. It is clear that $M_{O,2}$ contributes most to the total $M_O = M_{O,1} + M_{O,2} + M_{O,3}$, and thus, this improvement of $M_{O,3}$ is rarely considered. However, it could be considered automatically with our new algorithm. Adding up the contributions of the three components, the largest bond dimension always lies in the middle of the chain, which is $M_{O,\max} = 2(\frac{N}{2})^2 + 3(\frac{N}{2}) + 2$.

To consider the antisymmetry of fermions in the algorithm described in Sec. II B, the Jordan–Wigner transformation[62] for the elementary creation and annihilation operators is introduced,[6,33]

$$|\text{vacuum}\rangle = |\alpha\rangle, \quad (16)$$

$$|\text{occupied}\rangle = |\beta\rangle, \quad (17)$$

$$a^\dagger_j = \prod_{i=1}^{j-1} \sigma_z[i] \times \sigma_-[j], \quad (18)$$

$$a_j = \prod_{i=1}^{j-1} \sigma_z[i] \times \sigma_+[j]. \quad (19)$$

Figure 3(a) shows the maximal M_O of systems with 10–70 spin-orbitals, and Fig. 3(b) shows M_O at each bond of a system with 50

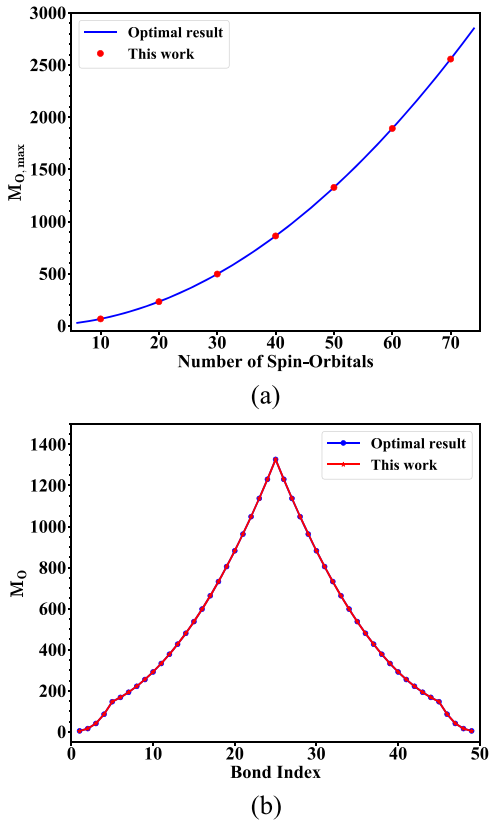

FIG. 3. (a) The maximal MPO bond dimension $M_{O,\max}$ of the *ab initio* electronic Hamiltonian with different numbers of spin-orbitals. The blue curve $M_{O,\max} = 2(\frac{N}{2})^2 + 3(\frac{N}{2}) + 2$ is the optimal result from the hand-crafted complementary operator strategy (see text for details). The red circles are the results obtained from the new automatic MPO construction algorithm. (b) The MPO bond dimension M_O at each bond of the *ab initio* electronic Hamiltonian of a 50 spin-orbital system.

19 November 2025 14:41:53

Published under license by AIP Publishing

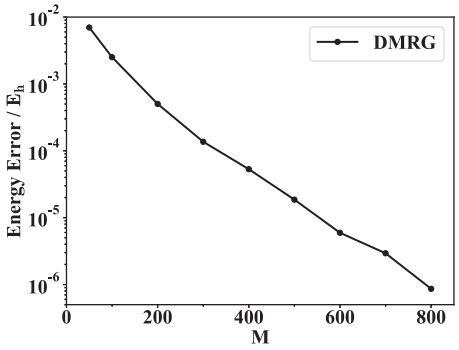

FIG. 4. The error of the ground state energy of H_2O with 6-31g basis calculated by the MPO based DMRG algorithm with different MPS bond dimensions M_S. The two-site algorithm is adopted to optimize the ground state MPS. The reference is the FCI energy $E_{FCI} = -76.119\,697\,04 E_h$. The MPO is generated by the new automatic MPO construction algorithm.

spin-orbitals. The correctness of the MPOs generated by the automatic algorithm has been verified by checking the residue $\|\mathrm{MPO}_1 - \mathrm{MPO}_2\| = 0$ with respect to the MPOs developed by Li and Chan in Ref. 6 and implemented in package QCMPO.[63] M_O at each bond and $M_{O,\max}$ (red asterisks) of the automatically generated MPO exactly match what the optimally hand-crafted strategy described above would give (blue circles), except that at the first bond, the automatic algorithm gives $M_O = 4$ ($\hat{W}[1] = [\sigma_-\sigma_+, \sigma_z\sigma_-, \sigma_z\sigma_+, \hat{I}]$), while the hand-crafted strategy gives $M_O = 5$ ($\hat{W}[1] = [h_{11}\sigma_-\sigma_+, \sigma_-\sigma_+, \sigma_z\sigma_-, \sigma_z\sigma_+, \hat{I}]$). The reason is the same as that in the case of Holstein models. In addition, in Fig. 3(b), M_O vs the bond index is symmetric as expected and the kink at the bond index 5 and 45 is due to the switch of the complementary operators from Eq. (15) to Eq. (14), indicating that the new algorithm could really find out the optimal solution.

We also calculate the ground state energy of the water molecule with 6-31g basis by the MPO-based DMRG algorithm. The structure of H_2O in the Cartesian coordinates is O(0, 0, −0.064 448 4), H(±0.749 915 1, 0, 0.511 491 3) in Angstroms. The electron integral and the reference full configuration interaction (FCI) result are calculated by PySCF.[64] The DMRG results with different M_S are shown in Fig. 4. The error of ground state energy with $M_S = 800$ is less than $1 \times 10^{-6} E_h$, which verifies the correctness of the MPO generated by the automatic algorithm.

C. Anharmonic vibrational Hamiltonian

The third example considered is the anharmonic vibrational Hamiltonian. There are two difficulties to solve the vibrational problems. One is how to calculate the matrix elements of high-dimensional PES, as introduced in Sec. I. The other is how to calculate the eigenstates or simulate the dynamics. Both of these two difficulties stem from the curse of dimensionality. To overcome the second difficulty, there have been a series of methods at different hierarchical levels, including vibrational self-consistent field (VSCF), vibrational perturbation theory (VPT), vibrational configuration interaction (VCI), vibrational coupled cluster (VCC), and multi-reference approaches.[38,65–69] (ML-)MCTDH combined with the improved relaxation algorithm[70] is another efficient method to obtain the eigenstates of the vibrational Hamiltonian. Recently, the DMRG has also been proposed to solve the anharmonic vibrational problem.[10–12] Herein, we use an approximate form of the Watson Hamiltonian in which only the second-order Coriolis terms are included,[11,71,72]

$$\hat{H} = \hat{H}_{\mathrm{vib}} + \hat{H}_{\mathrm{Cor}}, \tag{20}$$

$$\hat{H}_{\mathrm{vib}} = -\frac{1}{2}\sum_i \frac{\partial^2}{\partial q_i^2} + V(\{\boldsymbol{q}\}), \tag{21}$$

$$\hat{H}_{\mathrm{Cor}} = -\sum_\alpha B_\alpha \sum_{i<j}\sum_{k<l} \zeta_{ij}^\alpha \zeta_{kl}^\alpha \left(q_i \frac{\partial}{\partial q_j} - q_j \frac{\partial}{\partial q_i}\right) \times \left(q_k \frac{\partial}{\partial q_l} - q_l \frac{\partial}{\partial q_k}\right). \tag{22}$$

Here, B_α are the rotational constants and ζ_{ij}^α are the Coriolis coupling constants. In this numerical example, $V(\{\boldsymbol{q}\})$ is approximated as a sixth order Taylor expansion around the equilibrium geometry,

$$V(\{\boldsymbol{q}\}) = V_0 + \frac{1}{2}\sum_i \omega_i^2 q_i^2 + \frac{1}{3!}\sum_{ijk} F_{ijk} q_i q_j q_k + \frac{1}{4!}\sum_{ijkl} F_{ijkl} q_i q_j q_k q_l + \frac{1}{5!}\sum_{ijklm} F_{ijklm} q_i q_j q_k q_l q_m + \frac{1}{6!}\sum_{ijklmn} F_{ijklmn} q_i q_j q_k q_l q_m q_n. \tag{23}$$

It is a nontrivial task to construct a compact MPO of the operator in Eq. (23) because up to six sites are coupled together in a DMRG chain, more complicated than the *ab initio* electronic Hamiltonian. We note that two methods have been used to construct the MPO of this type of operator. In Ref. 10, a compact MPO is constructed by SVD compression, and in Ref. 11, a symbolic MPO is constructed in the second quantization formalism as the electronic Hamiltonian.[33] We will use the automatic MPO construction algorithm to demonstrate its effectiveness and generality. Although we use a PES expanded as a Taylor series in this example, it is worth mentioning that the algorithm is suitable to any PES expressed as an analytical SOP form. The molecule we choose is the widely studied C_2H_4 molecule.[11,12,65,72,73] The PES of C_2H_4 used here is a sextic force field as Eq. (23) from the PyPES library,[73] which is an adaptation of the PES constructed at the coupled-cluster single double and peturbative triple [CCSD(T)] level with quadruple-zeta basis in internal coordinates.[74] The constant V_0 is set to 0 for simplicity. Since C_2H_4 at equilibrium geometry has D_{2h} point group symmetry, there are only 2644 nonzero potential energy terms in the Hamiltonian otherwise it would be 18 485 terms. Figure 5 shows the MPO bond dimension at each bond of $\hat{H}_{\mathrm{vib}}$ of C_2H_4 with or without considering the point group symmetry. The 12 vibrational DoFs within the DMRG chain are arranged according to their harmonic frequencies ω_i. With point group symmetry, the largest MPO bond dimension is reduced from 112 to 77, which will reduce the computational cost spent in the DMRG static state or the time evolution calculations. Because the construction is automatic, the gain by utilizing symmetry to reduce the size of MPO is for free. Therefore, for

19 November 2025 14:41:53

Published under license by AIP Publishing

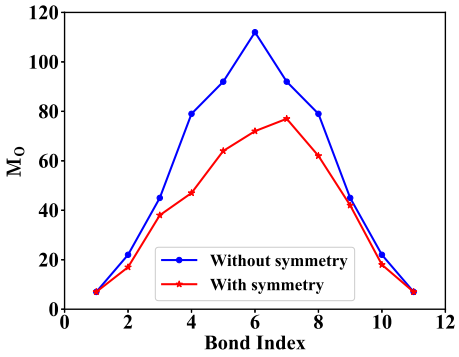

FIG. 5. The MPO bond dimension M_O vs bond index of C_2H_4 described by a sextic force field with or without considering D_{2h} point group symmetry.

the Hamiltonian with negligible terms, it would be efficient to use the current algorithm to construct the MPO after pre-screening the prefactors.

We use the linear response DMRG method under the Tamm–Dancoff approximation (DMRG-TDA) to calculate the vibrational excited states.[75,76] Compared to the other DMRG based algorithms for the high-lying excited states, such as DMRG with the shift-and-invert scheme,[12,77,78] DMRG with the folded operator,[12] and DMRG with projector and energy-shift,[11,26] the DMRG-TDA has the advantage that all the required eigenstates could be calculated in a single calculation and there is no need to track a specific state during the DMRG optimization procedure in order to avoid the root flipping problem.[12,79] To the best of our knowledge, it is the first time that the DMRG-TDA is applied to the vibrational correlation problem. In our calculation, the maximal occupation number (quanta) of each mode is limited to 6. The ground state is calculated by the state-averaged DMRG (SA-DMRG) for the lowest 9 states to make the renormalized basis more balanced for not only the ground state itself but also the excited states. Based on this ground state, we use the DMRG-TDA to calculate all the eigenstates below 4000 cm^{-1}. In Table I, we list the zero point energy, all 12 fundamental bands and the combination bands below 4000 cm^{-1} composed of a high-frequency C–H stretch and a low-frequency bend motion. The energy levels with or without considering the Coriolis coupling are both listed. Each DMRG-TDA wavefunction is compressed to a rank one Hartree product state to assign the main configuration in the correlated wavefunction. The label of each normal mode follows Ref. 74 and is listed in Table S1 of the supplementary material. For comparison, the VCI(8) results calculated by the PyVCI package[72] and the variational results reported in the literature[74] are also

TABLE I. The zero point energy (ZPE), 12 fundamental frequencies and 8 stretch–bend combination frequencies below 4000 cm^{-1} of C_2H_4 calculated by the DMRG-TDA.

	Without Coriolis term					With Coriolis term				
		DMRG-TDA				DMRG-TDA				
Assignment	Harmonic	$M_S = 50$	$M_S = 100$	$M_S = 200$	VCI(8)[a]	$M_S = 50$	$M_S = 100$	$M_S = 200$	VCI(8)[a]	Reference 74
ZPE	11 164.45	11 011.62	11 011.62	11 011.62	11 011.63	11 017.10	11 016.95	11 016.95	11 016.96	11 014.91
ν_{10}	824.97	820.25	820.01	819.99	820.11	823.69	823.55	823.53	823.66	822.42
ν_8	950.19	926.68	926.35	926.33	926.45	935.43	935.21	935.18	935.31	934.29
ν_7	966.39	942.03	941.68	941.65	941.78	950.89	950.64	950.61	950.74	949.51
ν_4	1 050.81	1 017.81	1 017.48	1 017.45	1 017.56	1 026.05	1 025.83	1 025.80	1 025.92	1 024.94
ν_6	1 246.76	1 222.41	1 222.17	1 222.15	1 222.23	1 224.91	1 224.81	1 224.79	1 224.87	1 225.41
ν_3	1 369.38	1 342.26	1 341.97	1 341.95	1 342.01	1 342.94	1 342.80	1 342.79	1 342.85	1 342.46
ν_{12}	1 478.48	1 438.61	1 438.33	1 438.31	1 438.39	1 441.90	1 441.77	1 441.76	1 441.84	1 441.11
ν_2	1 672.57	1 623.23	1 622.93	1 622.90	1 622.97	1 625.51	1 625.37	1 625.34	1 625.41	1 624.43
ν_{11}	3 140.91	2 978.69	2 978.09	2 978.01	2 978.20	2 985.73	2 985.35	2 985.28	2 985.48	2 985.38
ν_1	3 156.84	3 017.93	3 017.17	3 017.06	3 017.05	3 020.17	3 019.20	3 019.07	3 019.15	3 018.99
ν_5	3 222.89	3 072.75	3 071.86	3 071.20	3 071.51	3 079.63	3 079.27	3 079.17	3 079.36	3 079.86
ν_9	3 248.71	3 092.41	3 091.58	3 091.39	3 091.98	3 101.40	3 101.14	3 101.07	3 101.26	3 101.69
$\nu_{11} + \nu_{10}$		3 792.91	3 790.82	3 790.53	3 791.73	3 805.76	3 804.14	3 803.85	3 805.05	3 803.51
$\nu_1 + \nu_{10}$		3 831.52	3 828.88	3 828.57	3 829.80	3 836.10	3 834.30	3 834.02	3 835.17	3 833.27
$\nu_5 + \nu_{10}$		3 889.77	3 886.71	3 885.77	3 887.13	3 899.93	3 897.17	3 896.77	3 897.92	
$\nu_{11} + \nu_8$		3 902.58	3 897.06	3 897.02	3 897.86	3 926.18	3 914.00	3 914.03	3 914.74	3 912.73
$\nu_9 + \nu_{10}$		3 910.79	3 909.17	3 908.85	3 910.21	3 922.38	3 921.02	3 920.79	3 921.83	3 921.08
$\nu_{11} + \nu_7$		3 917.10	3 911.44	3 911.39	3 912.24	3 936.35	3 929.24	3 929.22	3 930.05	3 927.84
$\nu_1 + \nu_8$		3 936.71	3 937.59	3 936.20	3 931.12	3 952.56	3 943.27	3 942.03	3 944.20	3 946.68
$\nu_5 + \nu_8$		3 974.11	3 969.67	3 970.02	3 970.30	4 006.88	4 000.06	4 000.43	4 000.66	

[a]The VCI(8) results are calculated by package PyVCI from Refs. 72 and 73. VCI(8) means that up to 8 quanta could be excited in the CI calculation $\sum_i^N n_i \le 8$ (n_i is the number of quanta of the ith mode).

19 November 2025 14:41:53

Published under license by AIP Publishing

listed. Table I shows that the DMRG-TDA results have already converged within 1 cm^{-1} with only $M_S = 50$ for the fundamental bands. For the combination bands listed, the convergence within 1 cm^{-1} could be reached with $M_S = 100$, except the energy level $\nu_1 + \nu_8$ (<1.5 cm^{-1}). One of the reasons for this difference is that the DMRG-TDA is a single site excitation method on a correlated ground state reference. Thus, it is more efficient to target the fundamental bands than the combination bands. More sophisticated DMRG-CISD method,[75] in which the second-order tangent space of the MPS is also included, could further improve the accuracy of the combination bands. All the energy levels below 4000 cm^{-1} are listed in Table S2 of the supplementary material. The root mean square deviation of the DMRG-TDA results ($M_S = 200$) including the effect of Coriolis coupling compared to the available theoretical data in Ref. 74 is 0.74 cm^{-1} for the fundamental bands and 9.12 cm^{-1} for all bands below 4000 cm^{-1}. We expect that if the same form of PES is used, the deviation would be smaller. Although we choose a small molecule C_2H_4 as a numerical example here, the VDMRG is suitable for much larger molecules, such as that in Ref. 11, a peptide molecule is calculated.

Finally, we briefly discuss the computational scaling when using the MPO based DMRG algorithms. When dealing with the *ab initio* electronic Hamiltonian, it has been pointed out that directly treating the MPO as a dense matrix will result in an incorrect scaling $\mathcal{O}(N^5)$ compared to $\mathcal{O}(N^4)$ of the original DMRG algorithm in which only the renormalized operator matrix is retained.[33,49] The same problem will arise for the vibrational Hamiltonian with the sextic force field. The $M_{O,\max}$ of $\hat{H}_{\rm vib}$ with the number of vibrational modes is shown in Fig. 6 (blue curve). For $\hat{H}_{\rm vib}$, $M_{O,\max} = \frac{1}{48}N^3 + \frac{3}{8}N^2 + \frac{5}{3}N + 2$ when N is even. The leading term $\mathcal{O}(N^3)$ comes from the 3-index normal operators in each block, and the prefactor is $\binom{N/2}{3}$. When calculating the expectation value $\langle\Psi|\hat{H}|\Psi\rangle$ or optimizing the ground state, the cost spent in each blocking process is $\mathcal{O}(N^6)$ because the size of each local matrix in the MPO is $\mathcal{O}(N^3) \times \mathcal{O}(N^3)$. Hence, the total cost after each sweep is $\mathcal{O}(N^7)$. However, with the original DMRG algorithm, the bottleneck in the blocking process is to contract the 3-index normal operators $q_iq_jq_k$ in the L-block (R-block) and 1-index operator q_l in the center site to the complementary operator of q_mq_n in the R-block (L-block), which is $\hat{P}_{mn} = \sum_{ijk} F_{ijklmn}q_iq_jq_kq_l$, with a local computational scaling $\mathcal{O}(N^5)$ and in total $\mathcal{O}(N^6)$ in one sweep. To recover the correct scaling in the MPO based algorithm, two approaches have been proposed. One is to fully employ the sparsity of MPO when contracting tensors.[33] The other method is to split the total $\hat{H}_{\rm vib}$ into a sum of $\hat{H}_i$,[6,49] $\hat{H}_{\rm vib} = \sum_{i=1}^{N} \hat{H}_i$, where

$$\hat{H}_i = -\frac{1}{2}\frac{\partial^2}{\partial q_i^2} + V_0/N + \frac{1}{2}\omega_i^2 q_i^2 + \frac{1}{3!}\sum_{jk} F_{ijk}q_iq_jq_k + \frac{1}{4!}\sum_{jkl} F_{ijkl}q_iq_jq_kq_l + \frac{1}{5!}\sum_{jklm} F_{ijklm}q_iq_jq_kq_lq_m + \frac{1}{6!}\sum_{jklmn} F_{ijklmn}q_iq_jq_kq_lq_mq_n. \quad (24)$$

For $\hat{H}_i$ with index i fixed, the maximal 5-free-index operator will give an MPO with $M_{O,\max} = \mathcal{O}(N^2)$. The red curve in Fig. 6 shows $M_{O,\max}$ of $\hat{H}_i$ with the number of modes. The prefactor of the leading term is between $\frac{1}{4}$ and $\frac{1}{2}$. If all the N sub-MPOs are added up according to Eq. (7), the total MPO of $\hat{H}_{\rm vib}$ will be recovered with the same scaling of the bond dimension $\mathcal{O}(N^3)$, but with a larger prefactor. The advantage to introduce $\hat{H}_i$ is that the contraction of $\hat{H}$ could be first divided into contractions of $\hat{H}_i$ and then are summed up together. Even though the MPO of $\hat{H}_i$ is treated as a dense matrix, the computational scaling in the blocking process is $\mathcal{O}(N^4)$ for each of them, and the total N MPOs will result in $\mathcal{O}(N^5)$. Therefore, this "sum of MPO" algorithm not only recovers the correct computational scaling but also is easy to be parallelized.

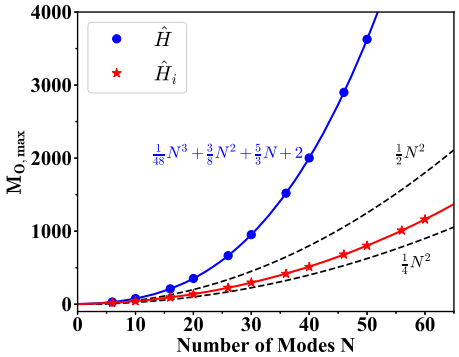

FIG. 6. The maximal MPO bond dimension $M_{O,\max}$ of the vibrational Hamiltonian $\hat{H}_{\rm vib}$ in Eq. (21) (blue circles) and $\hat{H}_i$ in Eq. (24) (red stars) vs the number of modes. The blue curve $\frac{1}{48}N^3 + \frac{3}{8}N^2 + \frac{5}{3}N + 2$ exactly fits the $M_{O,\max}$ of $\hat{H}_{\rm vib}$. The two black dashed curves $\frac{1}{4}N^2$ and $\frac{1}{2}N^2$ indicate that the scaling of $M_{O,\max}$ of $\hat{H}_i$ is $\mathcal{O}(N^2)$ and the prefactor is between $\frac{1}{4}$ and $\frac{1}{2}$.

IV. CONCLUSION AND OUTLOOK

In this work, we propose a new generic algorithm for the construction of the matrix product operator of any operator with an analytical sum-of-products form based on the bipartite graph theory. The most important feature of the algorithm is that it could translate the operator expression to the MPO representation automatically. Therefore, it is very useful for the current (TD-)DMRG methods to be easily extended to more problems described by different Hamiltonians. The idea of the new algorithm is to map the complementary operator selection problem to a minimum vertex cover problem in a bipartite graph, which could be elegantly solved by several well-established algorithms to get a locally optimal solution. We also prove that the constructed MPO is globally optimal. In addition, the new algorithm is symbolic and the sparsity of the Hamiltonian is fully preserved, which could be utilized to reduce the computational cost when contracting the tensors. We demonstrate the generality of the new algorithm by constructing MPOs ranging from the simple spin–boson model and the Holstein model to the more complicated *ab initio* electronic Hamiltonian and the vibrational Hamiltonian described by a sextic force field. In all of the examples, the new algorithm performs well in that it could find out the small redundancy in the near-optimal hand-crafted MPO, and

19 November 2025 14:41:53

Published under license by AIP Publishing

it could take advantage of the symmetry to reduce the dimension of MPO. Finally, one potential use-case of the presented algorithm not covered in the former examples is that if the coordinates system in the vibrational problem is curvilinear coordinates instead of normal mode rectilinear coordinates, the nuclear kinetic energy operators could be very complicated. The polyspherical approach developed by Gatti and co-workers[80,81] provides a general and analytical form of the kinetic energy operators expressed in terms of curvilinear coordinates, which often have thousands of summands and are very sensitive to numerical errors due to singularities. We expect that the symbolic feature of the current algorithm may be useful to contract the kinetic energy operators in these cases to reduce the computational cost when calculating the matrix elements.

SUPPLEMENTARY MATERIAL

See the supplementary material for the label of each normal mode of C_2H_4 and the energy levels below 4000 cm^{-1} calculated by the DMRG-TDA.

ACKNOWLEDGMENTS

J.R. thanks Hua Gu for insightful discussions on the graph theory and algorithm and also thanks Zhendong Li for critical reading of the manuscript and helpful comments. This work was supported by the National Natural Science Foundation of China through the project "Science CEnter for Luminescence from Molecular Aggregates (SCELMA)" (Grant No. 21788102) and by the Ministry of Science and Technology of China through the National Key R&D Plan (Grant No. 2017YFA0204501). J.R. was also supported by the Shuimu Tsinghua Scholar Program.

APPENDIX: PROOF OF THE GLOBAL OPTIMALITY

We will prove that sweeping from left to right with the procedure described in Sec. II B will not change the rank of the adjacency matrix at the same boundary. Starting from the left at the boundary between sites 1 and 2, after the first loop through steps 1–3, the coefficient matrix γ_1 is factorized as

$$\gamma_1 = \gamma_{z_1,z_2\cdots z_N} = \sum_{w_1} W[1]_{z_1,w_1} C[2:N]_{w_1,z_2z_3\cdots z_N}. \tag{A1}$$

The matrix $W[1]_{z_1,w_1}$ is the transformation matrix given in step 3. According to Lovász's theorem, the dimension of w_1, $|w_1|$, is equal to r_1. Equation (A1) is nothing but a special rank decomposition of matrix γ_1. Hence, both $W[1]$ (columns are linearly independent) and $C[2{:}N]$ (rows are linearly independent) have rank r_1. Thus,

$$C[2:N]_{w_1,z_2z_3\cdots z_N} = (W[1]^T W[1])^{-1} W[1]^T \gamma_1 = X[1]\gamma_1. \tag{A2}$$

We will show that the unfolding matrices of $C[2{:}N]$, which are $C[2:N]_2 = C[2:N]_{w_1z_2,z_3\cdots z_N}$, $C[2:N]_3 = C[2:N]_{w_1z_2z_3,z_4\ldots z_N}$, $\cdots$, and $C[2:N]_{N-1} = C[2:N]_{w_1z_2\cdots z_{N-1},z_N}$ all have rank$(C[2{:}N]_i) = r_i$. Since γ_i has rank r_i, a rank decomposition exists

$$\gamma_i = \gamma_{z_1\cdots z_i,z_{i+1}\cdots z_N} = \sum_{\beta=1}^{r_i} H_{z_1\cdots z_i,\beta} F_{\beta,z_{i+1}\cdots z_N}. \tag{A3}$$

Thus,

$$\begin{aligned} C[2:N]_i &= C[2:N]_{w_1z_2\cdots z_i,z_{i+1}\cdots z_N} \\ &= \sum_{z_1} X[1]_{w_1z_1} \gamma_{z_1z_2\cdots z_i,z_{i+1}\cdots z_N} \\ &= \sum_{z_1} X[1]_{w_1z_1} \left(\sum_{\beta=1}^{r_i} H_{z_1\cdots z_i,\beta} F_{\beta,z_{i+1}\cdots z_N} \right) \\ &= \sum_{\beta=1}^{r_i} \left(\sum_{z_1} X[1]_{w_1z_1} H_{z_1\cdots z_i,\beta} \right) F_{\beta,z_{i+1}\cdots z_N} \\ &= \sum_{\beta=1}^{r_i} M_{w_1z_2\cdots z_i,\beta} F_{\beta,z_{i+1}\cdots z_N}. \end{aligned} \tag{A4}$$

Therefore, rank$(C[2{:}N]_i) \le r_i$. On the other hand, if rank$(C[2{:}N]_i) < r_i$,

$$\begin{aligned} \gamma_i &= \sum_{w_1} W[1]_{z_1,w_1} C[2:N]_{w_1,z_2z_3\cdots z_N} \\ &= \sum_{w_1} W[1]_{z_1,w_1} \left(\sum_{\beta=1}^{\mathrm{rank}(C[2:N]_i)} M'_{w_1z_2\cdots z_i,\beta} F'_{\beta,z_{i+1}\cdots z_N} \right) \\ &= \sum_{\beta=1}^{\mathrm{rank}(C[2:N]_i)} \left(\sum_{w_1} W[1]_{z_1,w_1} M'_{w_1z_2\cdots z_i,\beta} \right) F'_{\beta,z_{i+1}\cdots z_N} \\ &= \sum_{\beta=1}^{\mathrm{rank}(C[2:N]_i)} H'_{z_1\cdots z_i,\beta} F'_{\beta,z_{i+1}\cdots z_N}. \end{aligned} \tag{A5}$$

The decomposition is contradictory to that the rank of γ_i is r_i. Thus, rank$(C[2{:}N]_i) = r_i$. The symbolic bipartite adjacency matrix between sites 2 and 3 is $C[2{:}N]_2$, which has rank r_2. $C[2{:}N]_2$ could be further symbolically decomposed by finding the maximum matching and then the transformation matrix in step 3,

$$C[2:N]_2 = \sum_{w_2=1}^{r_2} W[2]_{w_1z_2,w_2} C[3:N]_{w_2,z_3\cdots z_N}. \tag{A6}$$

The process can be continued by induction. This whole proof is very similar to Theorem 2.1 of Ref. 56. The difference is that the equality rank$(C[i{:}N]_j) = r_j$ $(j \ge i)$ always holds. The proof above could be intuitively understood from the fact that the rank of the coefficient matrix between two sub-systems will not change after sequential linear combinations of the basis in each sub-system as long as the new basis is linearly independent. Therefore, after sweeping from the left to the boundary between sites i and $i+1$, since the rank of the bipartite adjacency matrix $C[i{:}N]_i$ is r_i, the minimal number of retained operators is the same as the case that all normal operators are retained without any combination (complementary operators). As a result, the locally optimal solution is also globally optimal.

DATA AVAILABILITY

The data that support the findings of this study are available from the corresponding author upon reasonable request.

19 November 2025 14:41:53

Published under license by AIP Publishing

REFERENCES

[1] S. R. White, "Density matrix formulation for quantum renormalization groups," Phys. Rev. Lett. **69**, 2863 (1992).
[2] G. K.-L. Chan and S. Sharma, "The density matrix renormalization group in quantum chemistry," Annu. Rev. Phys. Chem. **62**, 465–481 (2011).
[3] J. Ren, Y. Yi, and Z. Shuai, "Inner space perturbation theory in matrix product states: Replacing expensive iterative diagonalization," J. Chem. Theory Comput. **12**, 4871–4878 (2016).
[4] Y. Ma, S. Knecht, S. Keller, and M. Reiher, "Second-order self-consistent-field density-matrix renormalization group," J. Chem. Theory Comput. **13**, 2533–2549 (2017).
[5] T. Yanai, M. Saitow, X.-G. Xiong, J. Chalupský, Y. Kurashige, S. Guo, and S. Sharma, "Multistate complete-active-space second-order perturbation theory based on density matrix renormalization group reference states," J. Chem. Theory Comput. **13**, 4829–4840 (2017).
[6] Z. Li and G. K.-L. Chan, "Spin-projected matrix product states: Versatile tool for strongly correlated systems," J. Chem. Theory Comput. **13**, 2681–2695 (2017).
[7] Z. Luo, Y. Ma, X. Wang, and H. Ma, "Externally-contracted multireference configuration interaction method using a DMRG reference wave function," J. Chem. Theory Comput. **14**, 4747–4755 (2018).
[8] A. Baiardi and M. Reiher, "The density matrix renormalization group in chemistry and molecular physics: Recent developments and new challenges," J. Chem. Phys. **152**, 040903 (2020).
[9] J. Brandejs, J. Višňák, L. Veis, M. Maté, Ö. Legeza, and J. Pittner, "Toward DMRG-tailored coupled cluster method in the 4c-relativistic domain," J. Chem. Phys. **152**, 174107 (2020).
[10] M. Rakhuba and I. Oseledets, "Calculating vibrational spectra of molecules using tensor train decomposition," J. Chem. Phys. **145**, 124101 (2016).
[11] A. Baiardi, C. J. Stein, V. Barone, and M. Reiher, "Vibrational density matrix renormalization group," J. Chem. Theory Comput. **13**, 3764–3777 (2017).
[12] A. Baiardi, C. J. Stein, V. Barone, and M. Reiher, "Optimization of highly excited matrix product states with an application to vibrational spectroscopy," J. Chem. Phys. **150**, 094113 (2019).
[13] E. Ronca, Z. Li, C. A. Jimenez-Hoyos, and G. K.-L. Chan, "Time-step targeting time-dependent and dynamical density matrix renormalization group algorithms with *ab initio* Hamiltonians," J. Chem. Theory Comput. **13**, 5560–5571 (2017).
[14] L.-H. Frahm and D. Pfannkuche, "Ultrafast *ab initio* quantum chemistry using matrix product states," J. Chem. Theory Comput. **15**, 2154–2165 (2019).
[15] S. M. Greene and V. S. Batista, "Tensor-train split-operator Fourier transform (TT-soft) method: Multidimensional nonadiabatic quantum dynamics," J. Chem. Theory Comput. **13**, 4034–4042 (2017).
[16] Y. Yao, K.-W. Sun, Z. Luo, and H. Ma, "Full quantum dynamics simulation of a realistic molecular system using the adaptive time-dependent density matrix renormalization group method," J. Phys. Chem. Lett. **9**, 413–419 (2018).
[17] J. Ren, Z. Shuai, and G. K.-L. Chan, "Time-dependent density matrix renormalization group algorithms for nearly exact absorption and fluorescence spectra of molecular aggregates at both zero and finite temperature," J. Chem. Theory Comput. **14**, 5027–5039 (2018).
[18] Y. Kurashige, "Matrix product state formulation of the multiconfiguration time-dependent Hartree theory," J. Chem. Phys. **149**, 194114 (2018).
[19] A. Baiardi and M. Reiher, "Large-scale quantum dynamics with matrix product states," J. Chem. Theory Comput. **15**, 3481–3498 (2019).
[20] X. Xie, Y. Liu, Y. Yao, U. Schollwöck, C. Liu, and H. Ma, "Time-dependent density matrix renormalization group quantum dynamics for realistic chemical systems," J. Chem. Phys. **151**, 224101 (2019).
[21] W. Li, J. Ren, and Z. Shuai, "Numerical assessment for accuracy and GPU acceleration of TD-DMRG time evolution schemes," J. Chem. Phys. **152**, 024127 (2020).
[22] W. Li, J. Ren, and Z. Shuai, "Finite-temperature TD-DMRG for the carrier mobility of organic semiconductors," J. Phys. Chem. Lett. **11**, 4930–4936 (2020).
[23] H.-D. Meyer, U. Manthe, and L. S. Cederbaum, "The multi-configurational time-dependent Hartree approach," Chem. Phys. Lett. **165**, 73–78 (1990).
[24] M. H. Beck, A. Jäckle, G. A. Worth, and H.-D. Meyer, "The multiconfiguration time-dependent Hartree (MCTDH) method: A highly efficient algorithm for propagating wavepackets," Phys. Rep. **324**, 1–105 (2000).
[25] H. Wang and M. Thoss, "Multilayer formulation of the multiconfiguration time-dependent Hartree theory," J. Chem. Phys. **119**, 1289–1299 (2003).
[26] H. R. Larsson, "Computing vibrational eigenstates with tree tensor network states (TTNS)," J. Chem. Phys. **151**, 204102 (2019).
[27] S. Östlund and S. Rommer, "Thermodynamic limit of density matrix renormalization," Phys. Rev. Lett. **75**, 3537 (1995).
[28] G. M. Crosswhite and D. Bacon, "Finite automata for caching in matrix product algorithms," Phys. Rev. A **78**, 012356 (2008).
[29] U. Schollwöck, "The density-matrix renormalization group in the age of matrix product states," Ann. Phys. **326**, 96–192 (2011).
[30] N. Nakatani and G. K.-L. Chan, "Efficient tree tensor network states (TTNS) for quantum chemistry: Generalizations of the density matrix renormalization group algorithm," J. Chem. Phys. **138**, 134113 (2013).
[31] K. Gunst, F. Verstraete, S. Wouters, Ö. Legeza, and D. Van Neck, "T3NS: Three-legged tree tensor network states," J. Chem. Theory Comput. **14**, 2026–2033 (2018).
[32] Z. Li, M. J. O'Rourke, and G. K.-L. Chan, "Generalization of the exponential basis for tensor network representations of long-range interactions in two and three dimensions," Phys. Rev. B **100**, 155121 (2019).
[33] S. Keller, M. Dolfi, M. Troyer, and M. Reiher, "An efficient matrix product operator representation of the quantum chemical Hamiltonian," J. Chem. Phys. **143**, 244118 (2015).
[34] J. Haegeman, C. Lubich, I. Oseledets, B. Vandereycken, and F. Verstraete, "Unifying time evolution and optimization with matrix product states," Phys. Rev. B **94**, 165116 (2016).
[35] L. Raff, R. Komanduri, M. Hagan, and S. Bukkapatnam, *Neural Networks in Chemical Reaction Dynamics* (OUP USA, 2012).
[36] B. Jiang and H. Guo, "Permutation invariant polynomial neural network approach to fitting potential energy surfaces," J. Chem. Phys. **139**, 054112 (2013).
[37] V. Barone, M. Biczysko, and J. Bloino, "Fully anharmonic IR and Raman spectra of medium-size molecular systems: Accuracy and interpretation," Phys. Chem. Chem. Phys. **16**, 1759–1787 (2014).
[38] V. Barone, "Anharmonic vibrational properties by a fully automated second-order perturbative approach," J. Chem. Phys. **122**, 014108 (2005).
[39] V. Barone, M. Biczysko, J. Bloino, M. Borkowska-Panek, I. Carnimeo, and P. Panek, "Toward anharmonic computations of vibrational spectra for large molecular systems," Int. J. Quantum Chem. **112**, 2185–2200 (2012).
[40] A. Jäckle and H. D. Meyer, "Product representation of potential energy surfaces," J. Chem. Phys. **104**, 7974–7984 (1996).
[41] D. Peláez and H.-D. Meyer, "The multigrid POTFIT (MGPF) method: Grid representations of potentials for quantum dynamics of large systems," J. Chem. Phys. **138**, 014108 (2013).
[42] F. Otto, "Multi-layer POTFIT: An accurate potential representation for efficient high-dimensional quantum dynamics," J. Chem. Phys. **140**, 014106 (2014).
[43] S. Manzhos and T. Carrington, Jr, "Using neural networks to represent potential surfaces as sums of products," J. Chem. Phys. **125**, 194105 (2006).
[44] S. Carter, S. J. Culik, and J. M. Bowman, "Vibrational self-consistent field method for many-mode systems: A new approach and application to the vibrations of CO adsorbed on Cu(100)," J. Chem. Phys. **107**, 10458–10469 (1997).
[45] E. L. Klinting, B. Thomsen, I. H. Godtliebsen, and O. Christiansen, "Employing general fit-bases for construction of potential energy surfaces with an adaptive density-guided approach," J. Chem. Phys. **148**, 064113 (2018).
[46] U. Manthe, "A time-dependent discrete variable representation for (multiconfiguration) Hartree methods," J. Chem. Phys. **105**, 6989–6994 (1996).
[47] U. Manthe, "A multilayer multiconfigurational time-dependent Hartree approach for quantum dynamics on general potential energy surfaces," J. Chem. Phys. **128**, 164116 (2008).
[48] G. Avila and T. Carrington, Jr, "Solving the Schrödinger equation using Smolyak interpolants," J. Chem. Phys. **139**, 134114 (2013).

19 November 2025 14:41:53

Published under license by AIP Publishing

[49]G. K.-L. Chan, A. Keselman, N. Nakatani, Z. Li, and S. R. White, "Matrix product operators, matrix product states, and *ab initio* density matrix renormalization group algorithms," J. Chem. Phys. **145**, 014102 (2016).
[50]T. Xiang, "Density-matrix renormalization-group method in momentum space," Phys. Rev. B **53**, R10445 (1996).
[51]C. Hubig, I. McCulloch, and U. Schollwöck, "Generic construction of efficient matrix product operators," Phys. Rev. B **95**, 035129 (2017).
[52]See https://github.com/shuaigroup/Renormalizer for Renormalizer.
[53]J. A. Bondy, U. S. R. Murty *et al.*, *Graph Theory with Applications* (Macmillan, London, 1976), Vol. 290.
[54]H. W. Kuhn, "The Hungarian method for the assignment problem," Nav. Res. Logist. Q. **2**, 83–97 (1955).
[55]J. E. Hopcroft and R. M. Karp, "An n^5/2 algorithm for maximum matchings in bipartite graphs," SIAM J. Comput. **2**, 225–231 (1973).
[56]I. V. Oseledets, "Tensor-train decomposition," SIAM J. Sci. Comput. **33**, 2295–2317 (2011).
[57]L. Lovász, "On determinants, matchings, and random algorithms," in *FCT* (Akademie-Verlag, 1979), Vol. 79, pp. 565–574.
[58]Ö. Legeza and J. Sólyom, "Optimizing the density-matrix renormalization group method using quantum information entropy," Phys. Rev. B **68**, 195116 (2003).
[59]G. Moritz, B. A. Hess, and M. Reiher, "Convergence behavior of the density-matrix renormalization group algorithm for optimized orbital orderings," J. Chem. Phys. **122**, 024107 (2005).
[60]M. Schröter, S. D. Ivanov, J. Schulze, S. P. Polyutov, Y. Yan, T. Pullerits, and O. Kühn, "Exciton–vibrational coupling in the dynamics and spectroscopy of Frenkel excitons in molecular aggregates," Phys. Rep. **567**, 1–78 (2015).
[61]T. Jiang, W. Li, J. Ren, and Z. Shuai, "Finite temperature dynamical density matrix renormalization group for spectroscopy in frequency domain," J. Phys. Chem. Lett. **11**, 3761–3768 (2020).
[62]P. Jordan and E. P. Wigner, "About the Pauli exclusion principle," Z. Phys. **47**, 631–651 (1928).
[63]See https://github.com/zhendongli2008/QCMPO for Qcmpo.
[64]Q. Sun, T. C. Berkelbach, N. S. Blunt, G. H. Booth, S. Guo, Z. Li, J. Liu, J. D. McClain, E. R. Sayfutyarova, S. Sharma *et al.*, "PySCF: The Python-based simulations of chemistry framework," Wiley Interdiscip. Rev.: Comput. Mol. Sci. **8**, e1340 (2018).
[65]O. Christiansen and J. M. Luis, "Beyond vibrational self-consistent-field methods: Benchmark calculations for the fundamental vibrations of ethylene," Int. J. Quantum Chem. **104**, 667–680 (2005).
[66]O. Christiansen, "Selected new developments in vibrational structure theory: Potential construction and vibrational wave function calculations," Phys. Chem. Chem. Phys. **14**, 6672–6687 (2012).
[67]C. Qu and J. M. Bowman, "Quantum approaches to vibrational dynamics and spectroscopy: Is ease of interpretation sacrificed as rigor increases?," Phys. Chem. Chem. Phys. **21**, 3397–3413 (2019).
[68]W. Mizukami and D. P. Tew, "A second-order multi-reference perturbation method for molecular vibrations," J. Chem. Phys. **139**, 194108 (2013).
[69]F. Pfeiffer and G. Rauhut, "Multi-reference vibration correlation methods," J. Chem. Phys. **140**, 064110 (2014).
[70]L. J. Doriol, F. Gatti, C. Iung, and H.-D. Meyer, "Computation of vibrational energy levels and eigenstates of fluoroform using the multiconfiguration time-dependent Hartree method," J. Chem. Phys. **129**, 224109 (2008).
[71]P. Carbonniere and V. Barone, "Coriolis couplings in variational computations of vibrational spectra beyond the harmonic approximation: Implementation and validation," Chem. Phys. Lett. **392**, 365–371 (2004).
[72]M. Sibaev and D. L. Crittenden, "PyVCI: A flexible open-source code for calculating accurate molecular infrared spectra," Comput. Phys. Commun. **203**, 290–297 (2016).
[73]M. Sibaev and D. L. Crittenden, "The PyPES library of high quality semi-global potential energy surfaces," J. Comput. Chem. **36**, 2200–2207 (2015).
[74]T. Delahaye, A. Nikitin, M. Rey, P. G. Szalay, and V. G. Tyuterev, "A new accurate ground-state potential energy surface of ethylene and predictions for rotational and vibrational energy levels," J. Chem. Phys. **141**, 104301 (2014).
[75]S. Wouters, N. Nakatani, D. Van Neck, and G. K.-L. Chan, "Thouless theorem for matrix product states and subsequent post density matrix renormalization group methods," Phys. Rev. B **88**, 075122 (2013).
[76]N. Nakatani, S. Wouters, D. Van Neck, and G. K.-L. Chan, "Linear response theory for the density matrix renormalization group: Efficient algorithms for strongly correlated excited states," J. Chem. Phys. **140**, 024108 (2014).
[77]J. J. Dorando, J. Hachmann, and G. K.-L. Chan, "Targeted excited state algorithms," J. Chem. Phys. **127**, 084109 (2007).
[78]X. Yu, D. Pekker, and B. K. Clark, "Finding matrix product state representations of highly excited eigenstates of many-body localized Hamiltonians," Phys. Rev. Lett. **118**, 017201 (2017).
[79]W. Hu and G. K.-L. Chan, "Excited-state geometry optimization with the density matrix renormalization group, as applied to polyenes," J. Chem. Theory Comput. **11**, 3000–3009 (2015).
[80]F. Gatti and C. Iung, "Exact and constrained kinetic energy operators for polyatomic molecules: The polyspherical approach," Phys. Rep. **484**, 1–69 (2009).
[81]M. Ndong, L. Joubert-Doriol, H.-D. Meyer, A. Nauts, F. Gatti, and D. Lauvergnat, "Automatic computer procedure for generating exact and analytical kinetic energy operators based on the polyspherical approach," J. Chem. Phys. **136**, 034107 (2012).

19 November 2025 14:41:53

Published under license by AIP Publishing